Fast Pyrolysis Kinetics of Expanded Polystyrene Foam

Pravin Kannan, Joseph J. Biernacki, and Donald P. Visco, Jr.
Dept. of Chemical Engineering, Tennessee Tech University, Cookeville, TN 38505

DOI 10.1002/aic.12092
Published online November 17, 2009 in Wiley InterScience (www.interscience.wiley.com).

Fast pyrolysis of polymers, biomass and other substances is of great interest in various applications. For example, in the lost foam casting process, kinetic information about expandable polystyrene (EPS) decomposition under extremely high-heating rate conditions is essential for further process development. A simple laboratory-scale fast pyrolysis technique has been developed and demonstrated for elucidation of EPS decomposition kinetics. Pyrolysis experiments were performed at different reaction temperatures. The cumulative gaseous yields were determined using a flame ionization detector (FID) connected in series with the fast pyrolysis reactor. The governing equations for a semibatch reactor type were modified and applied to obtain kinetic parameters (activation energies and the pre-exponential rate constants) for the EPS decomposition process. © 2009 American Institute of Chemical Engineers *AIChE J,* 56: 1569–1577, 2010
Keywords: polystyrene, reaction kinetics, polymer, foam properties

Introduction

The primary advantage of fast pyrolysis is extremely high-heating rates which elevate the sample to a target reaction temperature prior to complete volatilization. The main utility of the technique is that it enables decomposition to be observed at elevated temperatures that are otherwise difficult or impossible to attain with conventional techniques, such as thermogravimetry. Results obtained from fast pyrolysis are considered by others to be ''more generic, yet accurate'' and, hence, could be easily extended for various applications.[1] The basic underlying idea behind this technique is to rapidly take the sample to the elevated target temperature and minimize its exposure to the lower-temperatures that might influence the reaction sequence. In theory, this permits a more direct and simpler correlation between reaction rate and the process conditions, including thermal and environmental factors. Such a technique is demonstrated here for studying EPS decomposition kinetics and is discussed in the following sections.

Fast pyrolysis of expanded polystyrene foam (EPS) is of great interest to the lost foam casting industry wherein EPS forms are used to make metal castings. In metal casting environments, the foam may be heated at rates measured in 1000's °C/s. While some kinetics research has been done under casting-like conditions, new techniques for exploring the basic rate controlling mechanisms are still sought.

Correspondence concerning this article should be addressed to J. J. Biernacki at jbiernacki@tntech.edu.

Background of the Technique

A summary of the kinetic models and conventional experimental approaches available for EPS decomposition has already been published elsewhere,[2] whereas the following text briefly discusses literature findings on fast pyrolysis experimental techniques and kinetic data interpretation. *Fast* pyrolysis is ordinarily achieved by using a small amount of sample mass in a suitable form representative of the original and a very high-heating rate. Under such conditions, high rates of heat transfer and excellent instrumentation control are required to capture the dynamics of kinetic events that are later interpretable.

Liliedahl and Sjostrom[1] employed a laboratory-scale *fast* pyrolysis technique for the study of coal pyrolysis kinetics. Their design consisted of a pyrolysis chamber connected in series with a gas chromatograph that is fitted with a flame ionization detector. The pyrolysis chamber was a quartz tube packed with a small quartz wool plug to trap the sample.

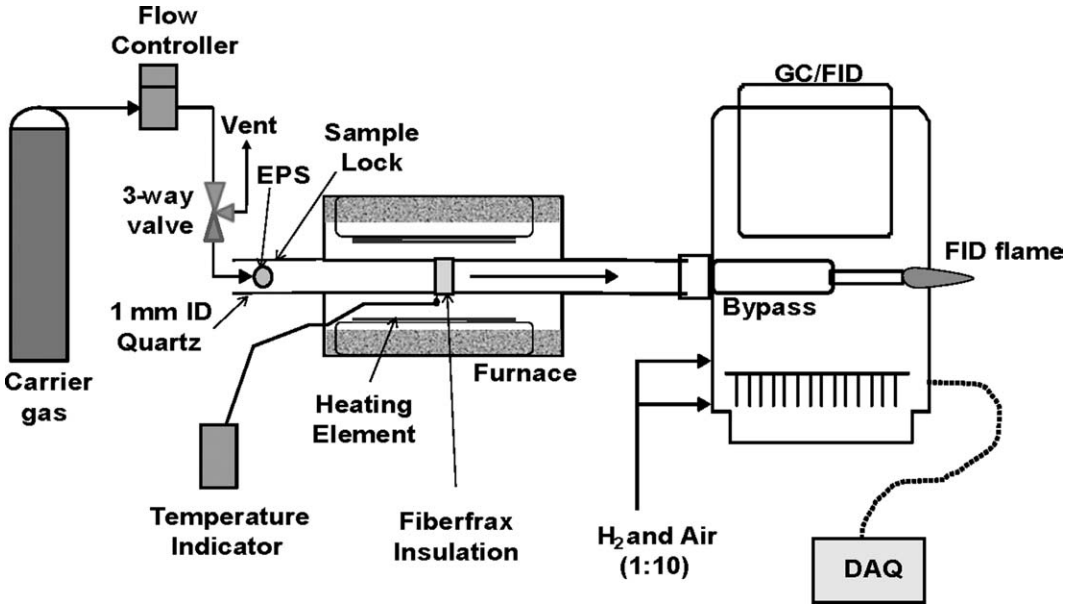

Figure 1. Experimental setup of the *fast* pyrolysis technique used in this study.

The quartz tube was placed inside a furnace that continuously heats the tube to maintain an isothermal condition. Coal samples in powder form were quickly introduced into the tube using a solids injector (entrainment by air). As the sample pyrolyzes, the carrier gas continuously sweeps the off-gas out of the furnace and into the chromatograph. Their chromatograph was slightly modified by replacing the lengthy GC capillary column with a short and empty column. This design facilitates transfer of the volatiles from the furnace exhaust port directly into the flame ionization detector (FID) with virtually zero residence time delay, limits the dispersion of the volatiles and does not obscure the fast reaction dynamics at the elevated temperatures.

The response of an FID is directly attributed to the mass of hydrocarbon molecules and the number of carbon-hydrogen bonds and is less sensitive to the carbon-oxygen bond, inert or halide group bonds. A carrier gas, usually an inert such as helium or nitrogen, ushers the pyrolysis off-gas through the "empty" GC and into the FID. Before the gas effluent enters the FID jet, it is mixed with hydrogen, making it combustible. It is then ignited in the presence of air into the FID where it produces both positive and negative ions. The negative ions are collected and the signal amplified, and a corresponding analog signal is generated that is recorded. The response from the FID represents a quantitative combined representation of both the mass and the number of hydrocarbon molecules eluted into the flame. The sensitivity of the instrument depends on several factors, including the stability of the flame. Hence, the ratio of air and hydrogen must be properly adjusted and maintained to provide the stable flame necessary for sample ionization.

To obtain relevant kinetic information, the FID data has to be processed so that it relates the reaction rate with time and temperature. Liliedahl et al.[1] monitored devolatilization rates over time at different isothermal temperature conditions and correlated the same to both single and multiple reaction kinetic models. Because coal samples pyrolyze via a complex set of multiple reactions, the kinetic approaches were found to be mathematically cumbersome. Hence, an empirical model was formulated based on a Gaussian distribution to relate the devolatilization rate to the instantaneous amount of volatile matter present in the effluent gas sample. By combining this model with an equation that incorporates the heat-transfer rate to the particle, the normalized total devolatilization rate as a function of pyrolysis time (t), and gas temperature (T) was derived

$$-\frac{dm'}{dt} = a\exp(bT)\left[\frac{2t^2}{a\exp(bT)t^4+2}\right]^{1.5} \quad (1)$$

where m' is the normalized volatile mass, and a and b are numerical rate constants that are specific for a given coal specimen.

Although this technique cannot be used to reveal the mechanistic details of the reaction, it suggests a useful methodology to correlate rate data based on the overall volatile yield.

Experimental Setup

The design of the pyrolysis apparatus is similar to the one employed by Liliedahl and Sjostrom[1], refer Figure 1, and consists of a tubular reactor that is connected in series with an FID equipped gas chromatograph. The tubular reactor is a 0.1 cm ID, 50 cm long quartz tube and a muffle furnace. Carrier gas (helium) from the storage cylinder flows into the reactor through a flow controller and a three-way valve. The carrier gas serves three purposes: (1) to transport a single EPS bead into the hot zone, (2) to transfer the volatiles from the reaction zone and into the FID, and (3) to provide a gaseous environment for the reaction. It is very important to choose a proper carrier gas-flow rate such that it not only minimizes the transfer time of both the sample and the volatiles, but also to provide a stable FID flame. After many

Table 1. Major Composition of the Hydrocarbon Gas Mixture Used as a Standard Test Gas in this Study

Component	Volume Fraction	Weight Fraction
Pentane	0.002	0.004
Pentene	0.002	0.004
Butane	0.002	0.004
Butene	0.004	0.007
Isobutane	0.103	0.188
Propane	0.007	0.010
Propylene	0.008	0.010
Ethane	0.020	0.019
Ethylene	0.020	0.018
Nitrogen	0.832	0.735

trials, a flow rate of 50 sccm was chosen for all the experimental runs.

Between the reactor and the flow controller, a three-way valve was installed. This permits gas to be diverted to vent while loading a sample into the sample lock, thus, maintaining a consistent upstream pressure. Upon sample injection, the three-way valve is switched so that gas flows through the reactor tube, thereby carrying the sample into the hot zone of the reactor. A small piece of Fiberfrax insulation was inserted into the quartz tube that serves to trap the EPS bead. The quartz tube was positioned inside the furnace such that the trap is in the middle of the furnace where the temperature is most uniform and highest. A *K*-type thermocouple was mounted on the top of the reactor tube just above the insulation trap to indicate the reaction temperature. For gas analysis, a *SRI Capillary FID GC* with *built-in* hydrogen generator was employed. The FID is equipped with an electrometer amplifier with adjustable gain. The *built-in* hydrogen generator option was not used in this study, and both air and hydrogen were supplied from an external storage tank to fuel the FID flame. The flow rates of air and hydrogen were controlled using the FID's electronic pressure controllers that were preset at a prescribed rate. The instrument has a wide detection range from 0.1 ppm to 100% for most hydrocarbons and can sample at a maximum rate of 50 Hz. The design inside the GC was slightly modified by replacing the entire GC capillary column with a short (ca. 25 cm) empty 1/16" OD stainless steel tube. One end of this tube was attached directly to the reactor quartz tube, and the other end connected to the injection port of the detector.

Expandable polystyrene beads or pre-expanded beads impregnated with pentane as a blowing agent were supplied by Styrochem, Inc. Nominally spherical EPS beads of about 0.5 mm dia. were selected and carefully weighed in a *TA Instruments SDT 2960* Simultaneous DSC-TGA. Although the balance sensitivity was on the order of 1 μg, disturbances from external factors limited the accuracy to about 5 μg. Under these circumstances, it was found that most of the selected EPS beads of the aforementioned dimensions weighed between 24 to 28 $\mu g \pm 5$ μg.

At the start of the experiment, the quartz tube was placed inside the furnace and heated to the target temperature. After obtaining a stable FID flame, a single EPS bead was placed in the lock at one end of the quartz tube as shown in Figure 1. This end is positioned far from the hot zone and so the temperature in the lock is not hot enough to initiate thermal changes in the sample. After attaining a stable carrier gas flow in the bypass line, the three-way valve was switched to permit flow into the reactor tube. The EPS bead is immediately carried into the reaction zone by the gas flow and trapped in the hot insulation wool where pyrolysis occurs. The volatiles that are formed are quickly transported out of the hot zone by the carrier gas and into the FID. The FID records the signal and transfers the data to the external data acquisition device.

Prior to the EPS pyrolysis runs, a set of control experiments were also conducted with a standard gaseous hydrocarbon mixture (see Table 1) in order to study dispersion and detector response dynamics as a function of furnace temperature and carrier gas-flow rate.

The total residence volume from the one end of the reactor tube to the FID jet was estimated to 1.13 mL. At a carrier gas flow rate of 100 sccm, the sample transit time from the sample lock to the FID flame is about 0.5 s. A simple experiment was performed to quantify the gas-phase dispersion in the reactor and transfer tube lines by injecting the gas standard at two different points along the stream. First, about 10 μL of the standard was injected through a septum into a flowing carrier gas stream with the use of a syringe near the sample lock ("Position 1" refer Figure 1. The 10 μL volume was chosen based on the theoretical total volatile yield of a single EPS bead pyrolyzed at 973 K. The yield of mixed gases from EPS pyrolysis at 973 K is about 200 mL per gram of EPS.[3] Assuming a bead mass of 45 μg (an upper limit), the total gas yield was calculated to be around 9 μL. Next, the experiment was repeated by injecting a sample at "Position 2" very close to the FID jet, and, hence, bypassing the entire reaction zone and transfer lines. The response curve of Position 1 is somewhat broader than that of Position 2 indicating some sample dispersion in the system. Since the actual kinetic event is expected to be at least one order of magnitude longer, the modest amount of dispersion shown here, will not significantly affect subsequent interpretations.

To study the effect of temperature on dispersion, the test gas was injected at Position 1 for three reactor temperatures, and the effluent was analyzed with the FID. The resulting FID response curves exhibited similar dynamics, thereby illustrating that temperature has little or no effect on the observed dispersion.

Since EPS volatilization temperatures range from 270 to 500°C, a series of pyrolysis experiments were conducted in and above this temperature interval. The entire experimental matrix is shown in Table 2. It was subsequently found that at temperatures below 465°C, the signal-to-noise ratio from the FID was very low, and, hence, a temperature range of 460–750°C was considered for kinetic study. This range

Table 2. EPS Pyrolysis Study Experimental Matrix (Including Preliminary Tests)

No.	Sample	Temperature (°C)	Test for
1	Test gas	Room	Dispersion
2	Test gas	515, 600, 735	Dispersion
3	EPS	463, 477, 478, 490, 500, 510, 549, 651, 707, 745	Pyrolysis tests
4	EPS	510	Reproducibility

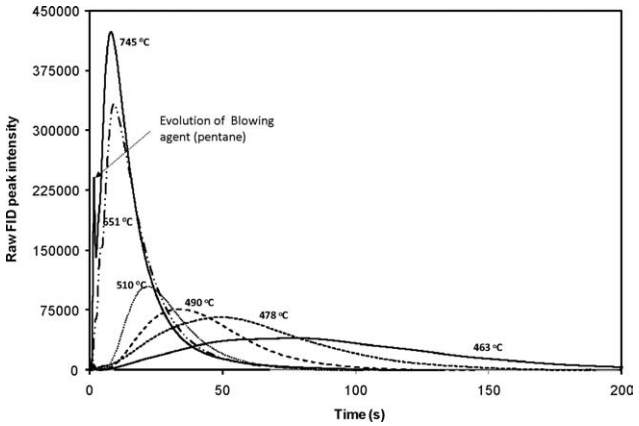

Figure 2. A comparison plot of FID *raw* peak intensities of EPS pyrolysis at different temperatures.

includes temperatures expected to be encountered in commercial aluminum casting processes since aluminum melts at about 660°C.

Results and Discussion

Figure 2 shows the *raw* (unprocessed) peak intensities collected using FID for EPS pyrolysis runs at different temperatures and Figure 3 shows the corresponding normalized FID peak intensities against pyrolysis time for various reactor temperatures. The normalized values for each temperature were calculated using the relationship $I^* = \frac{I - I_{\min}}{I_{\max} - I_{\min}}$ where I represents the raw peak intensity value at any time, and $I_{\min}$ and $I_{\max}$ represent the minimum and maximum peak intensities, respectively, at that particular temperature. The small peak noticeable during early reaction times (refer to Figures 2 and 3) corresponds to the evolution of the blowing agent (pentane) that is dissolved in the EPS during the synthesis step.

The raw peak intensity (ion current) detected by the FID at any instant is proportional to the number of carbon atoms present in the volatiles,[4] and the area under the curve between zero and time "t" is proportional to the cumulative amount of the volatiles generated by the pyrolysis reaction. By forming the ratio of the instantaneous value to the total area under the curve, the experimental reaction yield $Y(t)_{\exp}$ was computed

$$Y(t)_{\exp} = \frac{\int_0^t I(t)dt}{\int_0^\infty I(t)dt} \tag{2}$$

Since all pyrolysis experiments were conducted in a carrier flow of He, there will be no combustion products such as CO_2 or H_2O formed. It is possible, however, that small amounts of H_2 my form as the result of nonoxidizing carbon-hydrogen (C-H) bond cleavage. Since FID is not sensitive to H_2, the amount of H_2 formed would not be included in the total FID signal. This, however, is irrelevant since it is only necessary to quantify the amount of carbon present, which will be proportional to the fraction of EPS that went to form volatile pyrolysis products, regardless of the amount that might have gone to form H_2.

To test the repeatability of the experiment, three different pyrolysis runs were performed at reactor temperatures of 511°C, 513°C, and 518°C. It could be seen from Figures 4 and 5 that the variation between each run is minimal, and the deviations observed can likely be attributed to uncertainty in reaction temperatures. The experimental yield curves for various temperatures were constructed using Eq. 2, while the normalized derivative values in Figure 5 are estimated using the normalized intensity values as described earlier.

Prior to any interpretations, the relative variation of the area under the raw FID curves for different temperatures and the replicates were compared and analyzed. The area under the raw FID curve divided by the initial bead mass is proportional to the volatile product yield. Since the mass of an EPS bead used in all experimental runs is nominally constant, a plot of raw FID peak area vs. temperature is an indicator of how volatile yield varies with reaction temperature. Figure 6 shows a plot of total area under the curve estimated

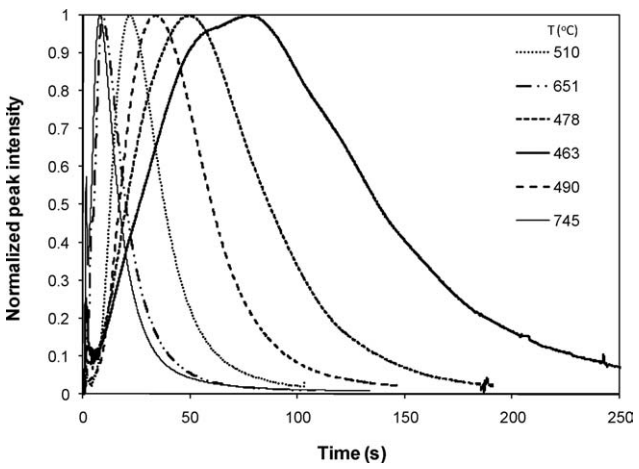

Figure 3. A comparison plot of normalized peak intensities of EPS pyrolysis at different temperatures.

The curve that is farthest to the left is the highest temperature (745°C), while that farthest on the right is for the lowest temperature (463°C).

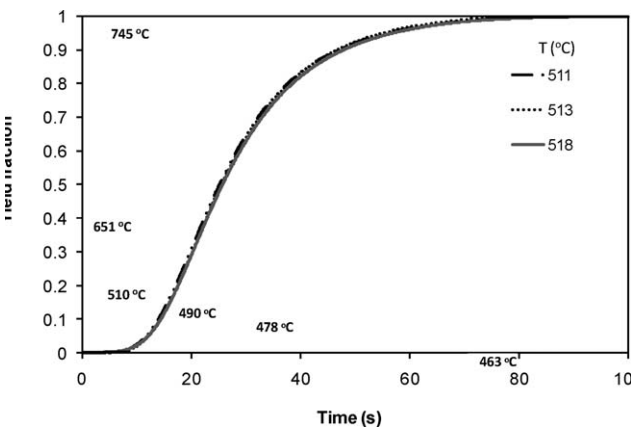

Figure 4. Reproducibility test; three different FID response curves at reactor temperatures of 511, 513 and 518°C.

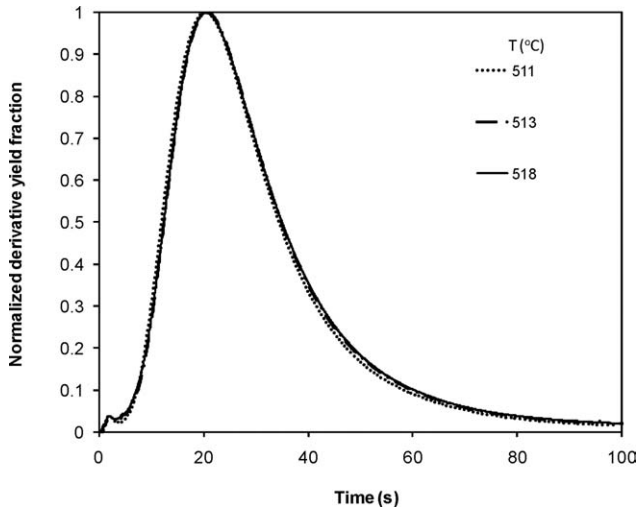

Figure 5. Reproducibility test; derivative of three different FID response curves at reactor temperatures of 511, 513 and 518°C.

using the denominator in Eq. 2 vs. reaction temperature. The error bar shown on the data point at a temperature at about 514°C is based on the statistical average of the three replicates at 511, 513, and 518°C. It could be concluded that the differences in area under the curves shown in Figure 2 for different temperatures are within the range of deviations between individual experimental runs although a suggestion of an increasing trend is noted. One might conclude that the volatile yield increases with reaction temperature, although the statistical confidence is low.

Figure 7 shows a plot of experimental yield fractions vs. time, parameterized by reaction temperatures between 463 and 651°C. Here, the reaction temperature is the temperature of the reaction chamber and is not necessarily the temperature of the sample. While these curves imply isothermal conditions, the shape of the pyrolysis curve is indicative of heat-transfer influence. At short times, all pyrolysis curves exhibit slow pyrolysis. During this period, the sample is heating, thus, pyrolysis is nonisothermal. This is more apparent at low-reactor temperatures. As reactor temperature increases, the maximum reaction rate increases until a reactor temperature of about 520°C as shown by the increasing slope of the yield vs. time curves. This observation is also indicative of heat transfer influences. A thorough discussion on the effects of heat-transfer phenomena is presented later.

For a single first-order reaction, a plot of $\ln(1/(1-Y(t))$ vs. time should yield a straight line. A plot of this test for yield fractions between 0.05 and 0.95 at various reaction temperatures is shown in Figure 8. The linearity of this relationship is evident from the value of the regression coefficient ($R^2 = 0.95$). Hence, it can be assumed that the entire reaction can be suitably modeled as a single first-order reaction.

The reactor system was modeled as a continuous stirred-semibatch reactor. Figure 9 shows a simplified illustration of the experimental reactor setup, wherein the solid lines represent the system, and the dotted lines represent the control volume. The notations V_R and T_R indicate the volume and temperature of the reactor, respectively. An overall mass balance on volume V_R for the system depicted in Figure 9 is represented by Eq. 3

$$\begin{array}{c}\textbf{Rate of mass}\\ \textbf{generated within}\\ \textbf{the reactor}\end{array} = \begin{array}{c}\textbf{Rate of mass}\\ \textbf{accumulated}\\ \textbf{within the reactor}\end{array} + \begin{array}{c}\textbf{Rate of mass out}\\ \textbf{from the reactor}\end{array} \tag{3}$$

Let $m_v(t)$ denote the instantaneous mass of total volatile content, and m_0 denote the initial mass of EPS. The mass-balance equation can then be expressed as shown

$$\left.\frac{dm_v(t)}{dt}\right|_{Rxn} = \left.\frac{dm_v(t)}{dt}\right|_{Acc} + \left.\frac{dm_v(t)}{dt}\right|_{Out} \tag{4}$$

The reaction rate for a single first-order reaction is expressed as a function of the mass of sample remaining

$$\left.\frac{dm_v(t)}{dt}\right|_{Rxn} = k(m_o - m_v(t)) \tag{5}$$

k is the Arrhenius rate constant that is assumed to follow an exponential relationship as shown in Eq. 6

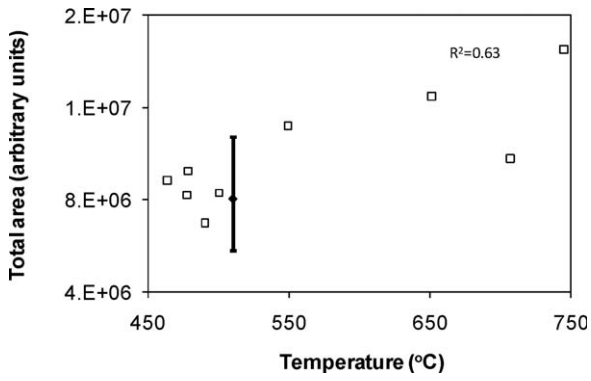

Figure 6. Comparison of total area under the FID curves at different temperatures experimental.

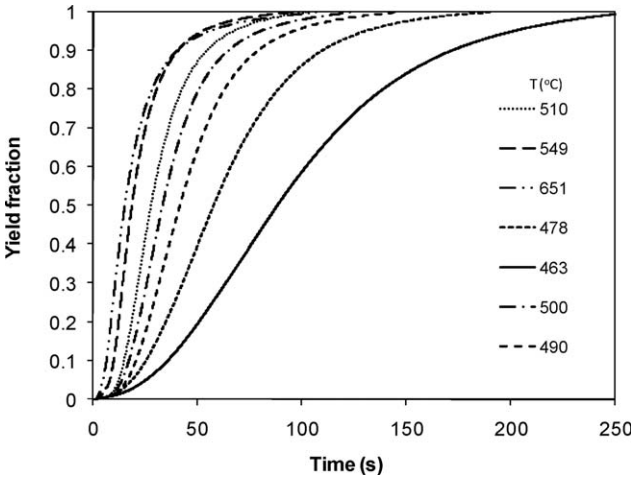

Figure 7. Experimental yields; fraction of volatiles at different reactor temperatures.

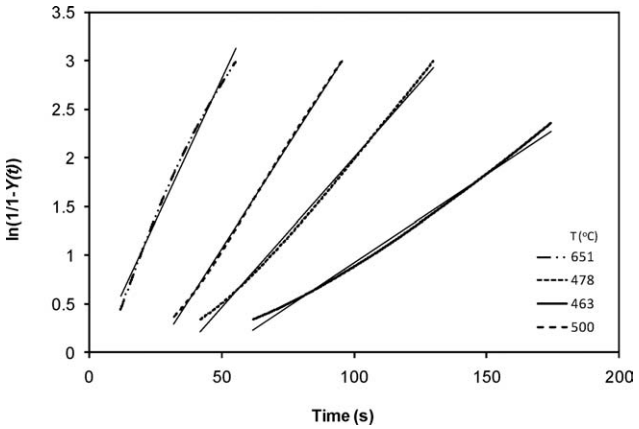

Figure 8. Validity test for single first-order reaction for conversion between 0.05 and 0.95.

$$k = A\exp\left(\frac{-E}{RT_s}\right) \tag{6}$$

The mass-outflow rate could be expressed as a function of $m_v(t)$, volumetric flow rate Q, and volume of the reactor V_R: $Qm_v(t)/V_R$. Finally, after substituting the individual terms into Eq. 4 the following differential equation (dynamic mass balance) is formed

$$\left.\frac{dm_v(t)}{dt}\right|_{Acc} = \left.\frac{dm_v(t)}{dt}\right|_{Out} - \left.\frac{dm_v(t)}{dt}\right|_{Rxn} = km_o - m_v(t)\left(\frac{Q}{V_R} + k\right) \tag{7}$$

If the theoretical yield is defined as $Y(t)_{\mathrm{mod}} = m_v(t)/m_o$, where the subscript "mod" is for "model," then upon integration, the analytical solution for $Y(t)_{\mathrm{mod}}$ is

$$Y(t)_{\mathrm{mod}} = \frac{-k}{k + Q/V_R}\left[-1 + \exp(-t(k + Q/V_R))\right] \tag{8}$$

Since it is not possible to determine the effective reactor volume (control volume) theoretically, the parameters k and V_R were optimized such that the objective function γ, defined as $\gamma = \frac{\sum_0^i \left(Y(t)_{\exp} - Y(t)_{\mathrm{mod}}\right)^2}{n}$ was minimized for each temperature, n being the total number of time steps (experimental observations).

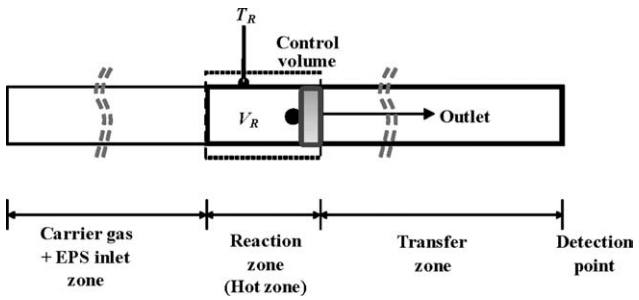

Figure 9. A simplified illustration of the experimental setup.

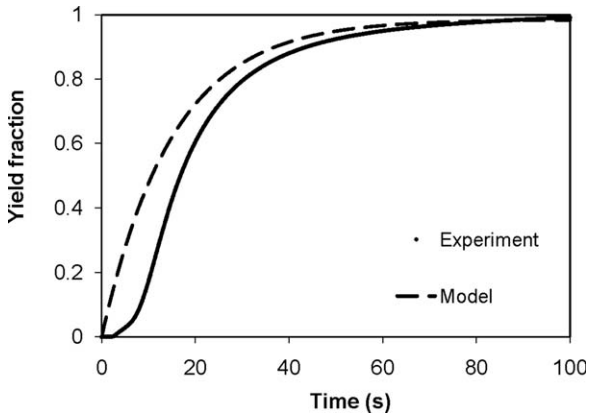

Figure 10. Comparison plot of experimental and isothermal model-based yield fractions for EPS pyrolysis at 750 K.

Figure 10 shows a comparison plot of the experimental and, the, thus, computed theoretical yield fraction of the volatiles pyrolyzed at a temperature of 750 K. Clearly, this model is not able to predict the decomposition behavior since it assumes isothermal conditions, and, hence, does not account for the heat-transfer effects occurring at early times. Therefore, it was necessary to account for the sample heat-transfer rate by incorporating appropriate heat-transfer equations into the overall kinetic model. Values of various parameters used for heat-transfer calculations have been tabulated (see Table 3).

The heat necessary for the pyrolysis reaction is transferred to the sample by combined gas-phase convection-conduction and radiation, and within the sample by solid phase conduction. In order to determine the dominating heat-transfer mechanism, both external and internal heat-transfer parameters were computed and compared.

Since the N_{Re} was less than 10 for all reaction temperatures, the temperature of the gas (T_g) surrounding the sample was calculated for fully developed laminar flow using the following equation[5]

$$\frac{T_w - T_g}{T_w - T_a} = 0.692e^{(-5.78\pi/Gz)} + .131e^{(-30.5\pi/Gz)} + 0.0534e^{(-74.9\pi/Gz)} + \ldots \tag{9}$$

where T_w is the wall temperature, T_a is the inlet gas temperature, and Gz is the Graetz number defined as follows

Table 3. Values of Various System and Thermal Parameters Used for Calculations

	EPS	Heater tube	Helium	Units
Diameters	0.0005	0.001	NA*	m
Thermal conductivities	0.03	NA	0.1713	W/m/K
Specific heats	1.3	NA	5193.2	J/kg/K
Emissivities	0.01	0.93	NA	Unitless
Vol. flow rate	NA	NA	0.83	cc/s
Densities	7	NA	0.173	Kg/m^3

*NA = not applicable.

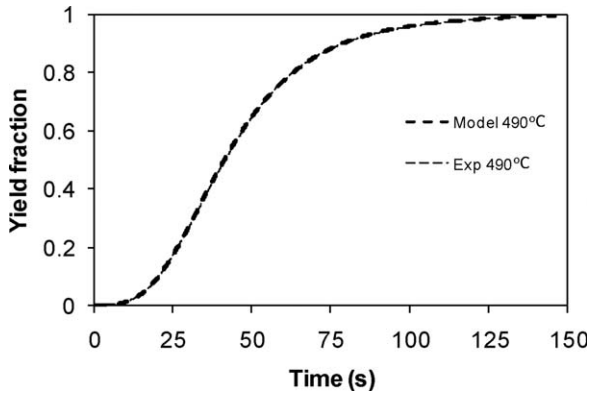

Figure 11. A comparison plot of nonisothermal model-based and experimental yield fractions at a reactor temperature of 763 K (490°C).

$$Gz \equiv \frac{Q\rho_g C_g}{k_g L} \tag{10}$$

where ρ_g is the gas density, C_g is specific heat capacity of the gas, k_g is the thermal conductivity of the gas, and L is the length of the hot section that was measured to be about 0.1 m. Based on the value of Graetz number and hot section length, the temperature of the gas phase around the sample was found to be equal to the wall temperature at all temperature conditions.

The convective heat-transfer coefficient (h_c) between a flowing fluid and the surface of a single spherical particle is given by[6]

$$\frac{h_c D_p}{k_g} = 2.0 + 0.60\left(\frac{D_p G}{\mu_g}\right)^{0.50}\left(\frac{C_p \mu_g}{k_g}\right)^{0.33} \tag{11}$$

where D_p represents the particle diameter, G is the mass velocity, and μ_g is the gas viscosity. Using the values shown in Table 3, the value of h_c was calculated to be about 700 W/m^2 K.

Assuming gray surfaces for both the quartz and the sample, the radiant heat-transfer coefficient (h_r) for $T_w \gg T_p$ is given by[7]

$$h_r = 4F\,\sigma_b T_w^3 \tag{12}$$

where σ_b is Stefan-Boltzman constant, and F is the overall interchange factor calculated using the individual emissivities (ε_1 and ε_2), and surface areas (A_1 and A_2) using the following relationship[8]

$$F = \frac{1}{1/\varepsilon_1 + \frac{A_1}{A_2}(1/\varepsilon_2 - 1)} \tag{13}$$

Assuming that the evaporating polystyrene behaves somewhat like a boiling film, the following correlation was applied to estimate the combined, convection-radiation heat-transfer coefficient

$$h = h_c\left(\frac{h_c}{h + h_r}\right)^{1/3} \tag{14}$$

The combined heat-transfer coefficient was computed for $Tp = 298$°C and when $T_p = T_w$, hence, hr $= 4\varepsilon\sigma_b T_w^3$ (from Eq. 12) and zero, respectively for the two extremes. From the computed values of heat-transfer coefficients, the Biot number was estimated to be in the range of 4–5 indicating an external heat-transfer controlled process. Hence the heat-transfer process seems to be dominated by combined gas-phase convection and radiation, and so radiative effects were included in all calculations, using T_p in all heat transfer calculations. Thus, the unsteady-state heat balance equation based on particle temperature is given by

$$m_p C_p \frac{dT_p}{dt} = h_c S\left(T_g - T_p\right) + S\varepsilon\sigma_b\left(T_w^4 - T_p^4\right) \tag{15}$$

where m_p is the mass of the particle, and S is the surface area of the particle. Solution of the unsteady-state heat balance equation for the particle yields a relationship for determining the average particle temperature (T_p) in terms of sample properties and heat-transfer coefficients[10]

$$T_p = T_a \exp(-Bt) + A(1 - \exp(-Bt)) \tag{16}$$

where the coefficients A and B are given by

$$A = \frac{h_c T_g + 4\varepsilon\sigma_b T_w^4}{h_c + 4\varepsilon\sigma_b T_w^3} \qquad B = \frac{S}{m_p C_p}\left(h_c + 4\varepsilon\sigma_b T_w^3\right) \tag{17}$$

Combining Eqs. 8, 9, and 16 and discretizing, the theoretical volatile yield was estimated by optimizing kinetic parameters, including activation energy and pre-exponential constant, reactor effective volume (V_R), and heat-transfer coefficient (h_r). Figure 11 shows a representative comparison plot of experimental and theoretical yield fraction as a function of time for a reaction temperature of 490°C. It can be seen

Table 4. Values of Kinetic Parameters, Heat-Transfer Coefficient, and Reactor Volume Estimated by Optimization with their Corresponding Standard Deviations Based on a 99% Confidence Interval

T_w (°C)	E (J/mol)	A (1/s)	h_c (W/m^{2}K)	V_R (cc)	R^2
463	25023 ± 13	41.6 ± .144	31 ± .06	.031 ± 4.4E-05	0.99
477	29360 ± 12	125.9 ± .186	52 ± .03	.027 ± 9.9E-07	0.99
478	29814 ± 17	120.7 ± .2	51. ± .05	.027 ± 4.2E-06	0.99
490	37516 ± 45	290.8 ± 1.41	97 ± .19	.028 ± 1.9E-05	0.99
500	41722 ± 194	412.2 ± 5.5	143 ± 1.3	.029 ± .0002	0.99
510	42623 ± 382	395 ± 6.3	182 ± 3.9	.031 ± .0006	0.99
511	37095 ± 329	238.6 ± 8.6	162 ± 2	.029 ± .0002	0.99
549	29045 ± 307	54.1 ± 1.3	194 ± 4	.028 ± .0001	0.99
651	17724 ± 81	6.07 ± .5	181 ± 7	.029 ± .0009	0.99
707	19094 ± 125	6.7 ± .5	189 ± 9	.029 ± .0008	0.99
745	13633 ± 125	3.12 ± .3	162 ± 7	.029 ± .0009	0.99

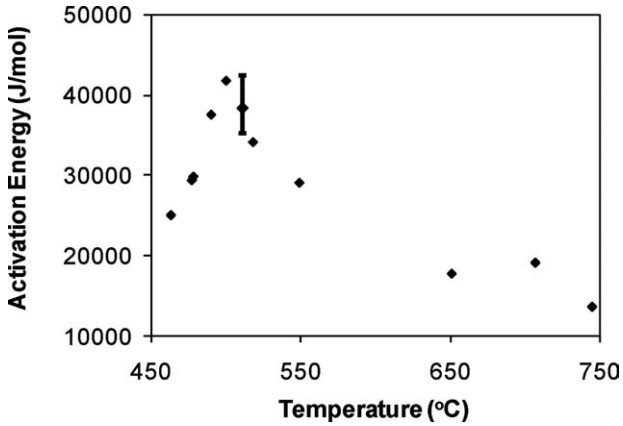

Figure 12. Variation of activation energy with reaction temperature — the error bar is ± one standard deviation for a triplicated experiment.

from the sample plot that the theoretical and experimental yield curves are in very good agreement. This is further evidenced by the values of the regression coefficient for all temperature conditions, refer Table 4. In all cases, the 99% confidence interval was constructed using Excel's nonlinear solver toolbox.

Figures 12 and 13 are an illustration of the variation of activation energy and heat-transfer coefficient, respectively, with respect to reaction temperature. The process seems to have relatively higher activation energy (ca. 35,000 J/mol) at low-temperatures compared to high-reaction temperatures (ca. 15,000 J/mol). At a first glance, the values of activation energy indicate that the process might be heat transfer controlled rather than reaction controlled. To test this case, the reaction functional form in Eq. 4 was modified from a simple first-order relation to one that is representative of a heat transfer controlled process (refer to the Appendix). At lower-temperatures, the resulting nonlinearity of the heat-transfer model disproves a heat transfer controlled process. However, at higher-temperatures, it seems that heat-transfer control is plausible since the model lines tend to be more linear. Hence, the overall decomposition process seems to be reaction-controlled phenomena only at lower-temperatures, and

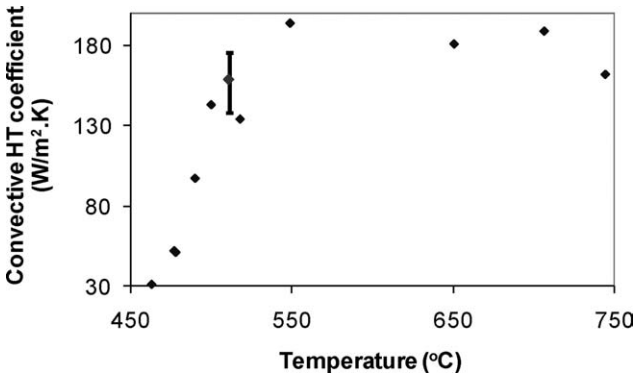

Figure 13. Variation of heat-transfer coefficient with temperature.

The error bars at 511°C represent experimental error calculated based on three replicates at nominally the same temperature.

Table 5. Standard Deviations of Kinetic Parameters, Heat-Transfer Coefficient, and Reactor Volume Based on Statistical Error and Experimental Error

	Average	Statistical Error	Experimental Error
Activation Energy (J/mol)	38295	329	3728
H.T. Coefficient (W/m^2-K)	158.6	2	19
Reactor volume (cc)	0.029	0.0002	0.002

may be heat transfer influenced at higher-temperatures. There is also a corresponding increase in the values of heat-transfer coefficient until 550 °C, after which it remains steady at about 180 W/m^2 K. The value of convective heat-transfer coefficient estimated from optimization is about four times smaller than theoretical predictions that were calculated to be about 700 W/m^2 K, likely due to correlation uncertainties for the given geometry and flow conditions.

In order to compare the relative scale of the statistical error (S.E) to the experimental error (E.E), standard deviations were calculated for the replicate runs at 511°C. It could be seen from Figures 12 and 13, and Table 5 that the experimental errors are higher than the statistical error. This difference could be mainly attributed to the sampling size over which the total errors are averaged. While the S.E is based on about 3,000 sample points, the E.E is averaged upon three individual experimental runs with slight variations in temperature and sample mass.

Notably, the activation energy values reported in this study are much lower than the ones reported in the literature[2] for EPS decomposition process. This is because most of the kinetic data presented in the literature, including those of the authors[12] were obtained from conventional thermal instruments where the heating rate is usually on the order of 50–100 K/min. In this study, the heating rate calculated based on the particle temperature is as high as 1200 K/min, and is on the order of 1000 K/min on an average, see Figure 14. This value was computed from the slopes during the nonisothermal heating period. These rates, however, are still low compared to those expected in lost foam casting environments which may be on the order of a few thousand degrees per second.[11]

It is a challenging task to design and fabricate a laboratory-scale reactor that is capable of delivering such high-

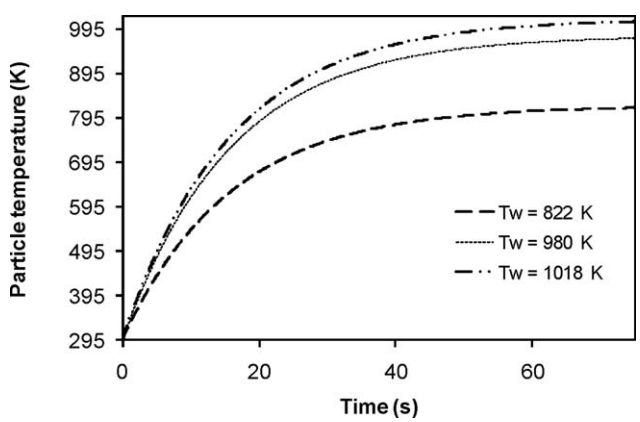

Figure 14. Predicted EPS sample temperature at various times during the reaction process for various constant reactor-wall temperatures.

heating rates as encountered in metal castings. Nevertheless, it could be noticed from the experimental yield curves, see Figure 8, that the reaction seems to proceed at a constant rate after a certain temperature, which is also indicated by very low-activation energies at these temperatures.

Finally, based on the reactor *effective* volume, the length of the actual reaction zone was estimated to be around 1 cm. This scale indicates that the EPS vaporization is very localized and located near the Fiberfrax insulation plug. This reduces the effects of any temperature variations that might be present along the axial length of the heater tube.

Conclusions

This study demonstrates a technique to study *fast* pyrolysis of EPS in a laboratory-scale environment. The entire experimental setup, including the reactor designed in this study seems a viable, simple and reliable apparatus for collecting experimental data at elevated temperature conditions with very little influence of the lower-temperature regions. Furthermore, a methodology for obtaining kinetic parameters, including activation energy and pre-exponential constant for EPS pyrolysis has been successfully demonstrated. Finally, by accounting for the heat-transfer coefficients and volumetric capacitance, the external effects on the kinetic parameters were minimized.

Acknowledgments

The authors would like to acknowledge financial support provided by Oak Ridge National Laboratory under subcontract #4000035322 entitled,"Counter Gravity (Hitchiner) and Pressure Assisted Lost Foam Magnesium Casting", and the Center for Manufacturing Research at the Tennessee Technological University.

Literature Cited

1. Liliedahl T, Sjostrom K. Modeling of coal pyrolysis kinetics. *AIChE J*. 1994;40:1515.
2. Kannan P, Biernacki JJ, Visco DP Jr. A review of physical and kinetic models of thermal degradation of expanded polystyrene and their application to the lost foam casting process. *J Anal App Pyrolysis*. 2007;78:162.
3. Bates CE, Griffin J, Littleton H. Expendable pattern casting-process manual. *AFS publication*. 1994;1:75.
4. Kuipers WJ, Muller J. A Planar micro-flame ionization detector with an integrated guard electrode. *J Micromech Microeng*. 2008;18:7.
5. McCabe WL, Smith JC, Harriott P. *Unit Operations of Chemical Engineering*. New York: McGraw-Hill; 2001:343.
6. McCabe WL, Smith JC, Harriott P. *Unit Operations of Chemical Engineering*. New York: McGraw-Hill; 2001:364.
7. McCabe WL, Smith JC, Harriott P. *Unit Operations of Chemical Engineering*. New York: McGraw-Hill; 2001:426.
8. McCabe WL, Smith JC, Harriott P. *Unit Operations of Chemical Engineering*. New York: McGraw-Hill; 2001:422.
9. McCabe WL, Smith JC, Harriott P. *Unit Operations of Chemical Engineering*. New York: McGraw-Hill; 2001:427.
10. Fan LS, Zhu C. *Principles of Gas-Solid Flows*. London, UK: Cambridge University Press; 1998:148.
11. Molibog T. *Experimental Modeling of the Metal/Pattern Exchange Mechanism in the Lost Foam Casting Process*. Birmingham, AL: University of Alabama; 1999. Thesis.
12. Kannan P, Biernacki JJ, Visco DP, Lambert W. Kinetics of thermal decomposition of expanded polystyrene in different gaseous environments. *J Anal Appl Pyrolysis*. 2008;84:139.

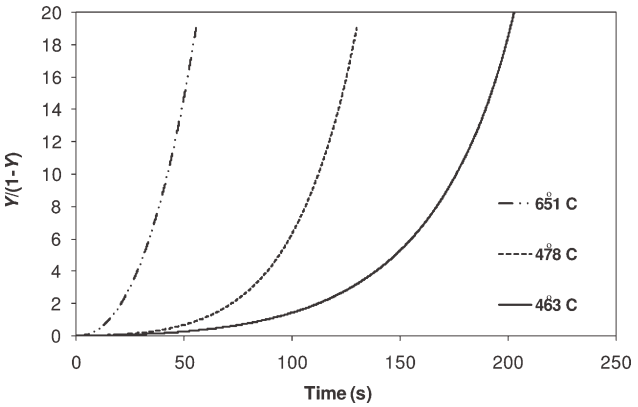

Figure A1. Plot of experimental Y values using a heat transfer controlled model.

Appendix

For a heat-transfer controlled process, the rate of volatile generation is given by

$$\frac{dm_v(t)}{dt} = \frac{h_c S}{\Delta H_r}\left(T_g - T_p\right) \tag{A1}$$

where ΔH_r is the endothermic heat of the reaction, S is the surface area of the particle, h_c is the heat-transfer coefficient, $m_v(t)$ is the mass of the volatiles at any instant t, T_g is the gas temperature and T_p is the particle temperature. In terms of yield fraction (Y), this can be written as

$$\frac{dY}{dt} = \frac{h_c \Delta T}{\Delta H_r}\frac{4\pi R_p(t)^2}{m_0} \tag{A2}$$

where $R_p(t)$ is the radius of the particle at any instant t, and m_0 is the initial mass of the sample.

Also

$$R_p(t) = R_0 Y \tag{A3}$$

where R_0 is the initial radius of the particle. Substituting for $R_p(t)$ in terms of Y in Eq. A2 yields

$$\frac{dY}{dt} = K'(1-Y)^2 \tag{A4}$$

where the constant K' is equal to $\frac{3h_c\Delta T}{R_0 \Delta H_r \rho_p}$.

Hence, for a heat transfer controlled process, a plot of (Y/($1-Y$)) against t for the experimental data should yield a straight line. Figure A1 shows poor linearity for such a relationship for three different temperatures of 463, 478 and 651°C.

Manuscript received Jun. 17, 2009, and revision received Aug. 20, 2009.